# Contrasting physical controls on subsurface phosphorus transport to shallow groundwater at different hillslope locations

Maëlle Fresne[1,2,3], Phil Jordan[2], Per-Erik Mellander[1,3], Karen Daly[3], Owen Fenton[3]

[1]Agricultural Catchments Programme, Teagasc, Johnstown Castle Environment Research Centre, Wexford, Co. Wexford, Ireland

[2]School of Geography and Environmental Sciences, Ulster University, Coleraine, UK

[3]Crops, Environment and Land Use Programme, Teagasc, Johnstown Castle Environment Research Centre, Wexford, Co. Wexford, Ireland

*Correspondence to:* M. Fresne (maelle.fresne@hotmail.fr)

## Abstract

In well-drained agricultural catchments water flow through the unsaturated zone (USZ) to shallow groundwater (GW), limiting soil phosphorus (P) attenuation, can be controlled by static and dynamic factors and contribute to elevated stream P concentrations. In order to better control P transport to GW at different hillslope locations, a spatial and temporal conceptual view of P transport through the USZ must be developed. Initially, hillslope GW quality and rainfall data were examined for 2017 utilising a transect of piezometers at midslope (MS) and downslope (DS) locations. Two dominant scenarios emerged where GW P concentrations at DS were variable and MS remained low or at other times DS remained elevated and MS remained low. To examine the potential physical reasons for such scenarios, a one-dimensional dual-porosity water flow model was developed for the USZ at DS and MS using rainfall and depth-specific soil hydraulic data determined from soil water retention curve modelling from undisturbed soil cores. Results indicated that the DS zone was 29 % less compacted, had a higher total porosity of 28 % (macroporosity of 13 %), a higher saturated water content of 25 % but a lower soil saturated hydraulic conductivity ($K_s$) of 62 % than the MS zone. This led to lower modelled cumulative water flow (74-78 % of total rainfall) compared to MS (76-80 %) and higher flow peaks during higher total rainfall events (4.1-5.2 mm $h^{-1}$ at DS, 3.5-4.9 mm $h^{-1}$ at MS). This suggested that water flow in the USZ is facilitated and P attenuation processes are more limited at DS during larger rainfall events contributing to higher GW P concentrations at DS, and is exacerbated with shallower GW mobilised soil P. Hence, mitigation strategies should particularly focus on reducing P sources in the DS zone but this also indicates a need to identify “hotspots” of facilitated water flow and P transport to shallow GW using finer scale soil properties surveys.

## 1. Introduction

Phosphorus (P) is a key nutrient for plant growth and food security (Cordell and White, 2014) but it can also be lost from agricultural land thereby contributing to the eutrophication of surface waters (Withers et al., 2014) which is a continuing global problem (Sinha et al., 2017). Within agricultural catchments, static (e.g. soil, subsoil and geology (Fenton et al., 2017)) and dynamic (e.g. climate (Mellander et al., 2018)) controls on P in groundwater (GW) and surface water are complex. Such controlling factors determine the timing, load, concentration and form of P delivered to a water body (Lintern et al., 2018). Concentrations of P in GW can be influenced by soil properties such as pH and clay % (Mabilde et al., 2017) as well as the presence of macropores or preferential flow paths (Bol et al., 2016; Julich et al., 2017; Fuchs et al., 2009). Bedrock P (sediments) and dissolution of P-rich minerals (McGinley et al., 2016) are also known as internal sources of P in GW. Temporal variations have been related to GW depth (Mabilde et al., 2017) influencing soil redox conditions and P release from Fe-oxides (Neidhardt et al., 2018; Dupas et al., 2015). Hydrological dynamics of hillslope shallow subsurface flows are highly variable in space and time (Bachmair et al., 2012b) and controlling factors include rainfall (Lehmann et al., 2007; Duan et al., 2017), bedrock topography and permeability (Tromp-van Meerveld and Weiler, 2008; Graham et al., 2010) as well as soil properties (Bachmair and Weiler, 2012a): topography (Bachmair and Weiler, 2012a), infiltration capacity, hydraulic conductivity, drainable porosity, moisture content and vertical and lateral preferential flowpaths (Guo et al., 2019; Anderson et al., 2009; Wilson et al., 1990, 2017).

To complement field studies on P transport, numerous models are available and conveniently cover a wide range of spatial (from soil profile (e.g., HGS, HYDRUS, PHREEQC) to catchment scale (e.g., SWAT)) and temporal scales (from days (e.g., ADAPT) to years)

(Pferdmanges et al., 2020). Water flow models first needs to be developed and validated to model P transport through the unsaturated zone (USZ). HYDRUS 1D is of particular interest for water transport to GW as it is one of the few models explicitly set up for simulations on short periods such as single rainfall events and focuses on vertical flux. Moreover, it offers a wide range of options to simulate preferential (macropore) flow (dual-porosity, dual-permeability models), important for P transport, and can be adapted to P using complex and numerous specific parameters values and transformation rates (Radcliffe et al., 2015). This model has been used to investigate the vertical distribution and transport processes of P (Elmi et al., 2012) or predict P leaching (Agah et al., 2016), for example.

Despite GW P being subject to microbial cycling, subsurface transport, and immobilization (Neidhardt et al., 2018), processes possibly attenuating belowground P, GW contribution to stream P is a concern (Mellander et al., 2016). This can be indicated by a higher contribution of bioavailable P (to total P) associated with a greater proportion of baseflow in rivers (Schilling et al., 2017). Therefore, any interpretation of contrasting P concentrations in GW at different monitoring points within a hillslope must include a variety of these factors. Increased characterisation and knowledge of contrasting scenarios is vital if best management practices on hillslopes are to be implemented correctly (i.e. right measure, right place) to safeguard water quality (Sharpley, 2016). Catchment scale studies with river and GW data, combined with physical data (meteorological and soil data, GW level), have the best opportunity to reveal transport processes from soils to GW and also subsequent delivery to surface water (Melland et al., 2012; Mellander et al., 2016; Mellander et al., 2014).

Combined field and laboratory techniques have used undisturbed (Bacher et al., 2019) or disturbed (Pang et al., 2016) soil, subsoil and bedrock samples that develop datasets to run model scenarios that best explain the transport of P to GW (Schoumans and Groenendijk, 2000; Schoumans et al., 2009). Different levels of data complexity (from simple to complex) affect transport model outcomes and it is therefore preferable where possible to collect undisturbed soil cores and develop soil physical and hydraulic parameters (Bünemann et al., 2018). Soil physical data such as porosity, saturated hydraulic conductivity ($K_s$) or bulk density ($\rho_b$), in combination with soil texture and water storage, can be used in models to assess water and solute transport dynamics through the USZ to GW (Fenton et al., 2015; Vero et al., 2014), in combination with site specific meteorological data (Gladnyeva and Saifadeen, 2013; Vero et al., 2014) and boundary conditions (Jacques et al., 2008; Vereecken et al., 2010). Combining high quality soil data with high resolution surface water, GW and meteorological data is an important approach towards a greater understanding of the major controls on P transport to shallow GW and thus provide important knowledge for GW P risk assessments. However, underground storage and release of P to GW and subsequent transit of P to surface water remains poorly understood (Gao et al., 2010).

The aim of this study was to address this knowledge gap and was undertaken in a meso-scale catchment observatory in Ireland with stream P dominantly delivered through below-ground pathways. Mellander et al. (2016) had previously showed that long-term dissolved reactive P (DRP) concentrations at the stream outlet were consistently above the Environmental Quality Standard (EQS) of 0.035 mg P $L^{-1}$. Initial testing of a multi-level borehole network in a connected hillslope revealed spatial and temporal fluctuations in P concentrations. Therefore, the present study examined the connected hillslope in greater detail with the objectives to:

1) investigate the effect of soil hydraulic properties on water flow and subsequent P transport through the USZ at different hillslope locations;

2) investigate the effect of dynamic physical controls (rainfall, GWL) on temporal variations in water flow and shallow GW P concentrations.

## 2. Materials and methods

### 2.1. Site description

The meso-scale agricultural catchment (7.58 $km^2$) (Fealy et al., 2010) is located in the south-west of Ireland (Co. Cork). A summary of catchment characteristics and long-term outlet concentrations of total dissolved P (TDP), DRP, dissolved unreactive P (DUP = TDP – DRP), iron (Fe) and dissolved organic carbon (DOC) are presented in **Table 1**. The catchment is dominated by well-drained soils (based on diagnostic features of the soil profile to 1 m and a soil survey at 1:25 000) and permeable bedrock, which results in high levels of infiltration and a groundwater-fed main river (Dupas et al., 2017a; Mellander et al., 2016).

Table 1: Summary of dominant catchment characteristics.

| | |
|---|---|
| **Average annual rainfall**[a] | 1 106 mm |
| **Average effective rainfall**[a] | 582 mm |
| **Soil type**[b] | Typical Brown Earth (Cambisol) and Typical Brown Podzols (Podzol) (84 %) |
| **Dominant Soil Drainage class**[c] | Well-drained |
| **Geology**[d] | Highly permeable sandstone, mudstone and siltstone |
| **Land use** | Grassland (84 %), Arable (6 %) |
| **Outlet water chemistry**[e] | 0.119 mg TDP $L^{-1}$, 0.078 mg DRP $L^{-1}$, 0.029 mg DUP $L^{-1}$, 0.41 mg Fe $L^{-1}$, 1.08 mg DOC $L^{-1}$ |

[a]Meteorological station located within the catchment see Figure 1, 2010-2016

[b]Irish classification system (World Reference Base classification system)

[c]Irish classification system (well-drained soil: no obvious sign of impeded drainage (mottling) throughout the solum. Exception where under pasture, sparse mottling may occur in topsoil)
[d]Geological Survey Ireland
[e]Monthly grab samples taken within the catchment see Figure 1, 2010-2016 (DOC 2012-2016)

The hillslope study site consists of a transect of piezometers screened in shallow bedrock and installed to monitor GW level and water quality at the downslope (DS) and midslope (MS) locations (**Fig. 1, Fig. 2**). Piezometer screen depths were 4-7 m at DS and 10.5-13.5 m at MS. Monthly grab samples were taken within the screen depth for chemical analysis using a 200 ml double valve bailer (Solinst, Canada). Samples were filtered (0.45 µm Sartorius) and TDP and DRP were analysed by spectrophotometry after alkaline persulphate oxidation (for TDP) (Askew, 2005) and after ascorbic acid reduction (for TDP and DRP) (method detection limit (MDL): 0.005 mg $L^{-1}$) (Askew and Smith, 2005). Dissolved unreactive P (DUP) was noted as the difference between TDP and DRP. Water level was recorded at high resolution using a Solinst water level logger to ascertain recharge. Average (2010-2016) depths to GW level (DGWL) were 0.30 ± 0.01 m at DS and 7.20 ± 0.28 m at MS.

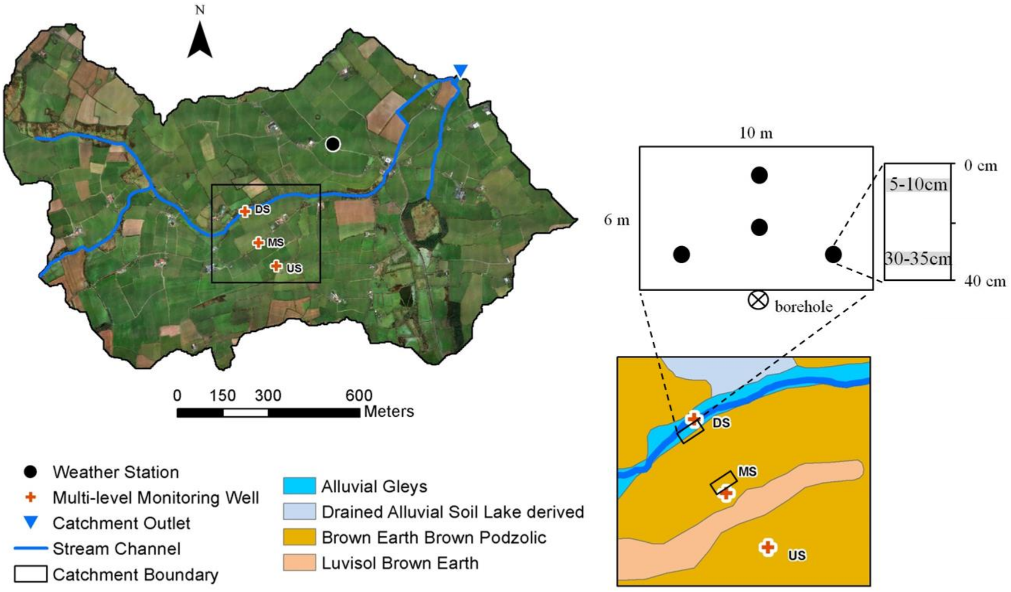


Figure 1: Location of the hillslope piezometers (DS, MS and US) within the context of the catchment, stream channel and outlet. The schematic on the lower right indicates soil types and intact coring location and depth of sampling around DS and MS.

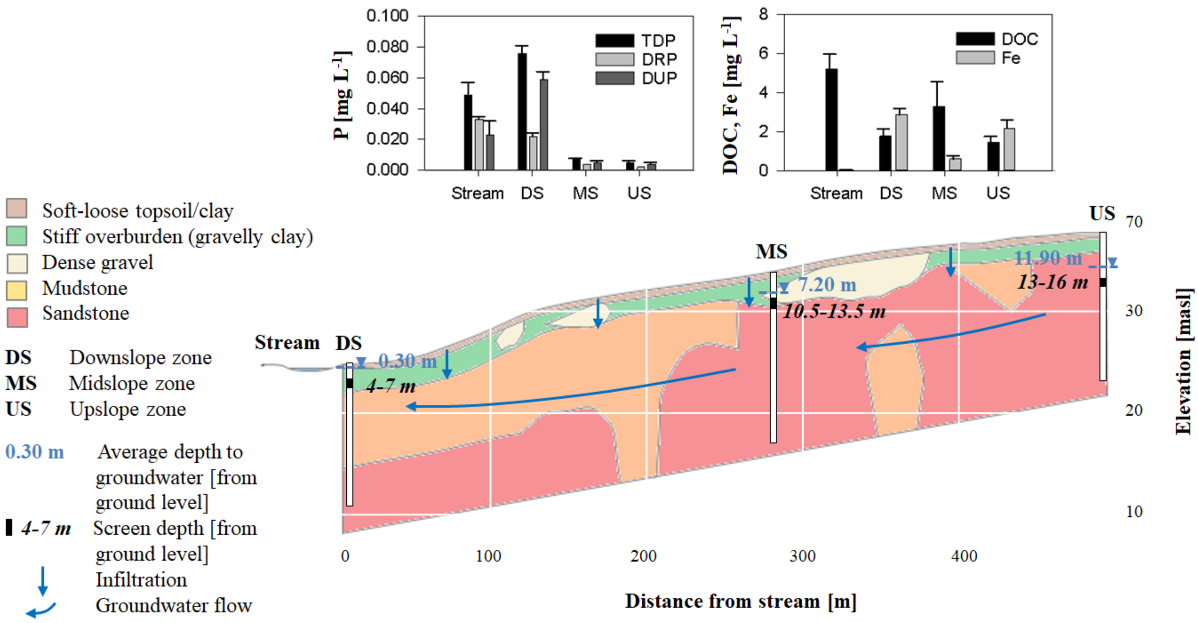


Figure 2: Geological cross section of the study hillslope showing the location of the piezometers (McAleer et al., 2017; Mellander et al., 2014). Also illustrated are the stream and

the groundwater chemistry at the study sites (based on monthly grab samples, 2010-2016 - DOC 2013-2016).

Using long terms datasets average concentrations of dissolved P and related parameters are shown in **Figure 2**. Site DS had higher P concentrations than at MS and in terms of DRP the stream data indicated long-term (2010-2016) average concentrations above or close to the EQS. It should be noted that there are soil type (based on 1 m depth only) differences at DS and MS/US with Alluvial Gley (Gleysol) and Typical Brown Earth/Podzols (Cambisol/Podzol), respectively.

### 2.2. Field methods - meteorological and soil data

For the purposes of the present study meteorological data taken from a Campbell Scientific BWS-200 weather station (**Fig. 1**) from January 2017 to December 2017 were examined. Absence of rainfall for at least 12 hours was used to separate one rainfall event from another (Ibrahim et al., 2013; Kurz et al., 2005) and only events having at least 5 mm rainfall were included in this process. These data were further sub-divided into 5 rainfall event types (A-E) depending on the total rainfall amount (A = 5.0-9.9 mm, B = 10.0-19.9 mm, C = 20.0-29.9 mm, D = 30.0-39.9 mm, E = ≥40 mm). Using the hybrid soil moisture deficit (SMD) model of Schulte et al. (2005) infiltration [mm] was estimated. Rainfall, infiltration and SMD data were used to develop modelling scenarios to investigate hydrological transport dynamics in the USZ at DS and MS locations.

Undisturbed soil cores (8 cm diameter, 5 cm height) were extracted at two depths (5 to 10 cm, 30 to 35 cm, 4 replicates) within a sampling grid close to DS and MS (**Fig. 1**). One additional soil core was taken at each site and depth. Using this strategy, 20 soil cores were collected between January and March 2018 before organic fertiliser (i.e. cattle slurry) was applied.

## 2.3. Laboratory methods

### 2.3.1. Undisturbed soil physical and hydraulic data

Soil $\rho_b$ [g cm$^{-3}$] was initially measured using the destructed additional soil cores and subsequently using the destructed undisturbed soil cores following soil physics hydraulic analysis. This was preferred to the direct determination via soil water retention curve (SWRC) analysis as results were distorted by the presence of stones in the undisturbed soil cores. Samples were oven-dried at 105 °C for 48 h and then weighed. Stones above 2 mm were extracted, weighed and their volume was determined. Soil $\rho_b$ was calculated by dividing the soil dry weight by the soil volume. Soil particle size distribution (PSD - sand, silt and clay content [%] (Brady and Weil, 2008)), using the pipette method (Avery and Bascomb, 1974), and soil texture were later determined using the 2 mm sieved soil from the additional soil cores.

The undisturbed cores were transferred to the laboratory for the continuous hydraulic measurement of a SWRC in terms of volumetric water content $\theta_v$ using an evaporation method. The Hyprop apparatus (UMS GmbH, Munich, Germany) (Bezerra-Coelho et al., 2018) was used for this purpose and a detailed procedure is described in Bacher et al. (2019). In summary, the raw Hyprop data from the direct SWRC approach were fitted to the bimodal van Genuchten model of Durner (Durner, 1994) - for the retention fitting - with the Mualem-constraint (Mualem, 1976) - for the $K_s$ fitting - which predicts the shape of the conductivity function from the shape of the retention function, to obtain the hydraulic parameters needed for the subsequent flow modelling. This dual-porosity model is a weighted superposition of two van Genuchten functions and is more suitable than the unimodal models to describe the retention functions of structured soils with bimodal pore-size characteristics. It also fitted better to the data than the unimodal constrained model of van Genuchten (1980). The detailed SWRC modelling steps and procedures are described in **S1** in the Supplement.

Hydraulic retention and conductivity parameters were then generated for each soil core: soil residual $\theta_r$ and saturated $\theta_s$ water contents [$cm^3$ $cm^{-3}$], soil $K_s$ [cm $d^{-1}$], SWRC shape parameters $n_1$ and $n_2$ [undimensional; -], $\alpha_1$ and $\alpha_2$ [$cm^{-1}$] and $\omega_2$ [-]. A statistical analysis ($E_{RMS}$) quantified the quality of the fits for both retention and conductivity.

To further interpret varied conditions at DS and MS additional parameters that could control transport to GW were calculated including total porosity $\phi$ [%], air capacity $\varepsilon$ [%], macro-, meso- and microporosity [%]. Detailed calculation steps are presented in **S2**. A list of abbreviations of soil physical and hydraulic parameters is presented in **Table 2**.

Table 2: List of abbreviations of soil physical and hydraulic parameters

| **Symbol** | **Abbreviation** |
|---|---|
| $\boldsymbol{\rho_b}$ | Bulk density |
| $\boldsymbol{\theta_r}$ | Residual water content |
| $\boldsymbol{\theta_s}$ | Saturated water content |
| $\boldsymbol{\alpha}$ | SWRC shape parameter: controls the air-entry pressure |
| $\boldsymbol{n}$ | SWRC shape parameter: controls the bending of the retention curve around the air-entry region and the curvature towards the residual water content |
| $\boldsymbol{K_s}$ | Saturated hydraulic conductivity |
| $\boldsymbol{l}$ | Pore connectivity |
| $\boldsymbol{\omega}$ | Weight of each van Genuchten sub-function |
| $\boldsymbol{\phi}$ | Total porosity |
| $\boldsymbol{\varepsilon}$ | Air capacity |

### 2.3.2. Modelling scenarios of water flow

Simulations were conducted using Hydrus 1D (Šimůnek et al., 2008; Šimůnek et al., 2013), coupled with appropriate meteorological and soil physical data, boundary conditions, and resulting water flow breakthrough curve at the bottom of the soil profiles was used to assess water transport dynamics through the USZ at DS and MS (**Fig. 3**).

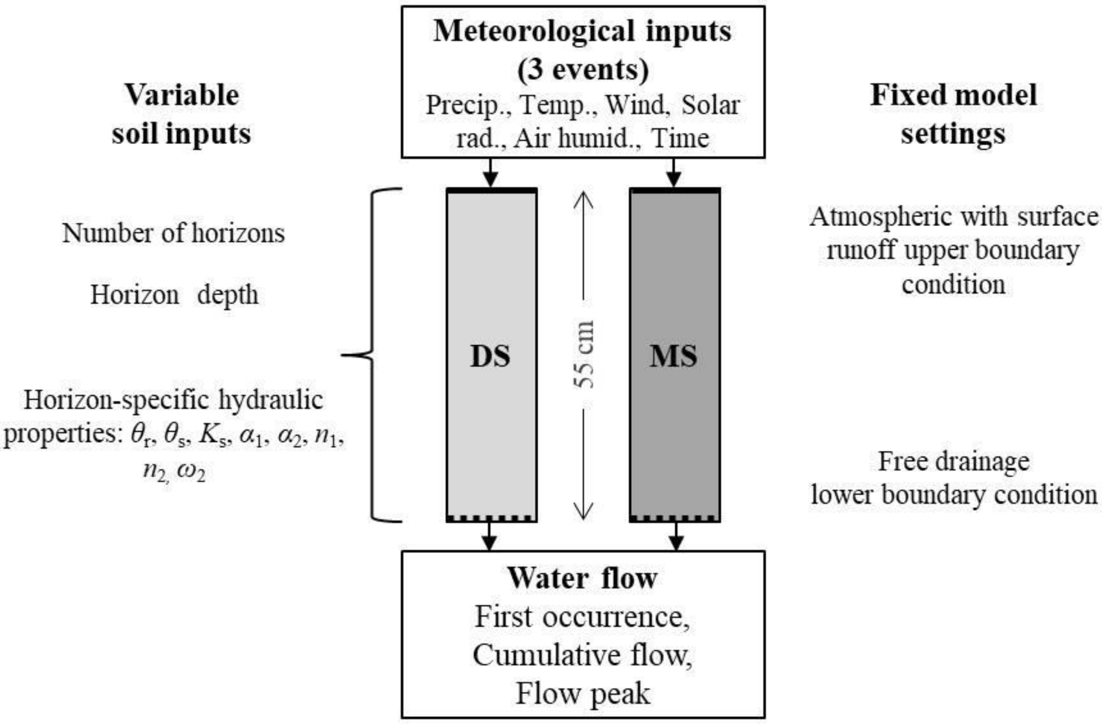


Figure 3: Conceptual diagram indicating input parameters, boundary conditions, soil horizon characteristics and model outputs.

Examination of soil profiles at both sites resulted in the delineation of soil horizons and the determination of the soil profile depths (55 cm for both sites). To build a soil profile for the dual-porosity model the physical and hydraulic data taken from the undisturbed soil cores were used for both DS and MS locations. Specifically $\theta_r$ and $\theta_s$ [cm$^3$ cm$^{-3}$], $K_s$ [cm h$^{-1}$], SWRC shape parameters $\alpha_1$ and $\alpha_2$ [cm$^{-1}$], $n_1$ and $n_2$ [-], and $\omega_2$ [-] were used as input parameters. Median values of soil physical and hydraulic parameters (**Table 3**) were used to choose the replicate which was the most representative of the site and depth. Choice was first based on the $K_s$ value which was deemed to be the most critical for water transport, then on $\theta_s$ when two replicates were similarly close to the median value. Hydraulic data of the selected soil core were applied to the soil horizon including this soil core sampling depth and, when no hydraulic data were available for a horizon, the data from the upper horizon were applied. Soil pore connectivity parameter $l$ was set at 0.5 [-] following the original study by Mualem (1976). To determine initial soil moisture conditions along the soil profiles for the subsequent transient flow modelling, steady-state flow was first modelled. A constant water flux of 0.0068 cm $h^{-1}$ (average annual infiltration (precipitation – potential evaporation) over the period 2010-2017 in the study catchment) with free drainage was applied on both soil profiles at DS and MS.

To investigate the effect of variable rainfall conditions on water flow through the USZ, transient flow was later modelled at the bottom of the soil profiles at DS and MS with one model run carried out for each contrasting (in terms of total rainfall and duration) rainfall event (R1, R2 and R3) leading to six model scenarios in total. The model was started at the beginning of the rainfall event and was ended the hour preceding the beginning of the following rainfall event. Atmospheric upper boundary conditions with surface runoff were assigned to the model in order to examine the role of soil hydraulic properties and rainfall patterns on water transport. The contrasting rainfall events were expected to affect water transport dynamics differently (and subsequently chemical P attenuation processes). Hourly (Vero et al., 2014) total precipitation (cm), maximum and minimum temperatures [ºC], average wind speed [km $d^{-1}$], average solar radiation [MJ $cm^{-2}$] and average air humidity [%] data from 2017 were used as input parameters. Free drainage was specified as the lower boundary condition (Jacques et al., 2008).

### 2.4. Data and statistical analysis

For objective 1, descriptive statistics of soil parameters were carried out for each depth and site. Soil $K_s$ values with $E_{RMS} > 0.90$ were removed for this purpose as they were deemed to be not representative of the soil core. Analysis of variance (ANOVAs) was later used to investigate significant ($P < 0.05$) differences of soil properties between depths within each site and between sites for each depth. Residual plots were used to assess the normal distribution of the residuals and the equal variance of the data; data were log transformed before statistical analyses when those conditions were not met. Trends were studied when the variation between replicates was very high (e.g. $K_s$). Pearson R correlations were used to measure the degree of relationship between soil parameters. Statistical analysis was carried out using R Studio 3.5.2.

## 3. Results

### 3.1. Soil hydraulic properties

Detailed soil physical and hydraulic data for all undisturbed soil core replicates of sites DS and MS are shown in Tables **S3** and **S4**, respectively. Descriptive statistics of soil physical and hydraulic parameters for each depth and site are shown in **Table 3**. Below is a description of the overall (at the scale of the sampling area, including the four replicates) variations observed between sites and depths. Soil at DS is a Sandy Loam whereas MS soil has a Loamy texture.

Median soil $\rho_b$ was higher (not significantly) at MS than DS for both shallow and deeper soil cores. Soil $\rho_b$ increased with depth (not significantly) in each site: from 0.85 to 0.95 g $cm^{-3}$ at

DS, and from 1.22 to 1.28 g $cm^{-3}$ at MS. Soil organic matter content (OM %) was higher at DS (8.3 %) than at MS (4.6 %).

Median soil $\theta_r$ was equal to 0 $cm^3$ $cm^{-3}$ for shallow soil at DS and at MS while it was equal to 0.06 $cm^3$ $cm^{-3}$ in deeper soil at DS. Median soil $\theta_s$ was higher (not significantly) at DS than MS for both shallow and deeper soil cores. Soil $\theta_s$ decreased with depth (not significantly) in each site: from 0.64 to 0.59 $cm^3$ $cm^{-3}$ at DS, and from 0.54 to 0.47 $cm^3$ $cm^{-3}$ at MS.

At both sites and for both depths, soil $K_s$ was variable. Median $K_s$ was higher (not significantly) at DS than MS for shallow soil cores and higher at MS than DS for deeper soil cores. Soil $K_s$ decreased with depth (not significantly) at each site: from 1914 to 209 cm $d^{-1}$ at DS, and from 1866 to 1468 cm $d^{-1}$ at MS.

Median $\phi$ was higher (not significantly) at DS than MS for both shallow and deeper soil cores. Soil $\phi$ decreased with depth (not significantly) at each site: from 68 to 64 % at DS, and from 54 to 51 % at MS. Median $\varepsilon$ was higher (not significantly) at DS than MS for both shallow and deeper soil cores. Soil $\varepsilon$ increased with depth (not significantly) at each site: from 21 to 26 % at DS, and from 14 to 19 % at MS.

Median soil macroporosity was higher (not significantly) at DS than MS for both shallow and deeper soil cores. Soil macroporosity significantly decreased with depth at MS - from 43 to 39 % - but not significantly at DS - from 50 to 41 %. Median soil mesoporosity and microporosity were comparable between DS and MS for both shallow and deeper soil cores, and both decreased with depth.

Soil $\rho_b$ was strongly and significantly correlated to sand (R = - 0.828), silt (R = 0.792) and clay % (R = 0.833) as was soil $\phi$ (R = 0.828, R = - 0.794, R = - 0.829, respectively). Soil air capacity $\varepsilon$ was correlated to clay % (R = - 0.503).

Table 3: Descriptive statistics of soil hydraulic parameters for DS and MS

| Site | Depth | | $\rho_b$ | $\alpha_1$ | $n_1$ | $\alpha_2$ | $n_2$ | $\omega_2$ | $\theta_r$ | $\theta_s$ | $K_s$ | $\phi$ | macro | meso | micro | $\varepsilon$ |
|---|---|---|---|---|---|---|---|---|---|---|---|---|---|---|---|---|
| | | | g $cm^{-3}$ | $cm^{-1}$ | - | $cm^{-1}$ | - | - | $cm^3$ $cm^{-3}$ | $cm^3$ $cm^{-3}$ | cm $d^{-1}$ | % | % | % | % | % |
| DS | 5-10 cm | AVERAGE | 0.89 | 0.292 | 2.743 | 0.103 | 1.313 | 0.630 | 0.03 | 0.63 | 2197[a] | 66 | 49 | 6 | 2 | 22 |
| | | MEDIAN | 0.85 | 0.334 | 1.643 | 0.010 | 1.259 | 0.638 | 0.00 | 0.64 | 1914[a] | 68 | 50 | 6 | 2 | 21 |
| | | MAX | 1.05 | 0.500 | 6.267 | 0.391 | 1.486 | 0.822 | 0.13 | 0.69 | 4110[a] | 69 | 53 | 9 | 3 | 28 |
| | | MIN | 0.80 | 0.002 | 1.418 | 0.002 | 1.248 | 0.423 | 0.00 | 0.55 | 567[a] | 60 | 43 | 5 | 1 | 18 |
| | | SD | 0.10 | 0.216 | 2.040 | 0.166 | 0.100 | 0.142 | 0.06 | 0.05 | 1460[a] | 4 | 4 | 2 | 1 | 4 |
| | 30-35 cm | AVERAGE | 0.95 | 0.365 | 1.460 | 0.149 | 1.353 | 0.687 | 0.10 | 0.58 | 829 | 64 | 40 | 4 | 1 | 24 |
| | | MEDIAN | 0.95 | 0.392 | 1.336 | 0.047 | 1.342 | 0.674 | 0.06 | 0.59 | 209 | 64 | 41 | 4 | 1 | 26 |
| | | MAX | 1.04 | 0.500 | 2.159 | 0.500 | 1.591 | 0.943 | 0.27 | 0.63 | 2892 | 67 | 50 | 6 | 3 | 36 |
| | | MIN | 0.86 | 0.177 | 1.010 | 0.001 | 1.135 | 0.459 | 0.00 | 0.51 | 7 | 60 | 28 | 1 | 0 | 9 |
| | | SD | 0.06 | 0.140 | 0.440 | 0.206 | 0.164 | 0.177 | 0.11 | 0.04 | 1201 | 2 | 8 | 2 | 1 | 10 |
| MS | 5-10 cm | AVERAGE | 1.20 | 0.139 | 1.376 | 0.174 | 1.438 | 0.490 | 0.00 | 0.55 | 2981 | 54 | 45 | 6 | 2 | 14 |
| | | MEDIAN | 1.22 | 0.118 | 1.376 | 0.097 | 1.408 | 0.503 | 0.00 | 0.54 | 1866 | 53 | 43 | 7 | 2 | 14 |
| | | MAX | 1.31 | 0.320 | 1.522 | 0.500 | 1.738 | 0.630 | 0.00 | 0.67 | 7762 | 59 | 53 | 8 | 3 | 17 |
| | | MIN | 1.07 | 0.001 | 1.231 | 0.001 | 1.198 | 0.326 | 0.00 | 0.47 | 431 | 50 | 40 | 4 | 1 | 9 |
| | | SD | 0.10 | 0.140 | 0.115 | 0.203 | 0.237 | 0.109 | 0.00 | 0.08 | 2835 | 4 | 5 | 2 | 1 | 3 |
| | 30-35 cm | AVERAGE | 1.27 | 0.250 | 1.239 | 0.012 | 1.545 | 0.525 | 0.07 | 0.48 | 2990[b] | 51 | 35 | 4 | 1 | 19 |
| | | MEDIAN | 1.28 | 0.250 | 1.274 | 0.001 | 1.564 | 0.463 | 0.00 | 0.47 | 1468[b] | 51 | 39 | 4 | 1 | 19 |
| | | MAX | 1.40 | 0.500 | 1.400 | 0.047 | 1.753 | 0.904 | 0.27 | 0.52 | 6464[b] | 57 | 43 | 6 | 2 | 22 |
| | | MIN | 1.12 | 0.000 | 1.010 | 0.000 | 1.298 | 0.269 | 0.00 | 0.44 | 1038[b] | 46 | 18 | 0 | 0 | 15 |
| | | SD | 0.10 | 0.181 | 0.145 | 0.020 | 0.168 | 0.236 | 0.12 | 0.03 | 2463[b] | 4 | 10 | 2 | 1 | 2 |

[a]Without replicate 3 for which $E_{RMS}$ $K_s$ = 0.9046

[b]Without replicate 2 for which $E_{RMS}$ $K_s$ = 0.9291

Soil physical and hydraulic data used as input parameters in Hydrus 1D are presented in **Table 4**. Spatial variations (between depths and sites) in soil parameters used as input variables were in accordance with the overall tendencies observed and described previously.

Table 4: Summary of soil hydraulic data used as input parameters in Hydrus 1D.

| **Site** | **Horizon depth** | $\boldsymbol{\theta_r}$ | $\boldsymbol{\theta_s}$ | $\boldsymbol{\alpha_1}$ | $\boldsymbol{n_1}$ | $\boldsymbol{K_s}$ | $\boldsymbol{l}$ | $\boldsymbol{\omega_2}$ | $\boldsymbol{\alpha_2}$ | $\boldsymbol{n_2}$ |
|---|---|---|---|---|---|---|---|---|---|---|
| | | $cm^3$ $cm^{-3}$ | $cm^3$ $cm^{-3}$ | $cm^{-1}$ | - | cm $h^{-1}$ | - | - | $cm^{-1}$ | - |
| **DS** | 0-23 cm | 0.00 | 0.63 | 0.500 | 1.816 | 80 | 0.5 | 0.618 | 0.004 | 1.256 |
| | 23-43 cm | 0.00 | 0.60 | 0.284 | 1.174 | 17 | 0.5 | 0.610 | 0.001 | 1.591 |
| | 43-55 cm | 0.00 | 0.60 | 0.284 | 1.174 | 17 | 0.5 | 0.610 | 0.001 | 1.591 |
| **MS** | 0-25 cm | 0.00 | 0.57 | 0.320 | 1.522 | 94 | 0.5 | 0.630 | 0.004 | 1.214 |
| | 25-55 cm | 0.00 | 0.48 | 0.500 | 1.400 | 61 | 0.5 | 0.516 | 0.001 | 1.298 |

### 3.2. Rainfall events, soil moisture deficit, water table depth and groundwater quality

Rainfall during 2017 is presented in **Figure 4a**. During that year 56 rainfall events were categorised as follows: 18 events A, 21 events B, 6 events C, 9 events D and 2 events E (Table **S5**, A = 5.0-9.9 mm, B = 10.0-19.9 mm, C = 20.0-29.9 mm, D = 30.0-39.9 mm, E = ≥40 mm).

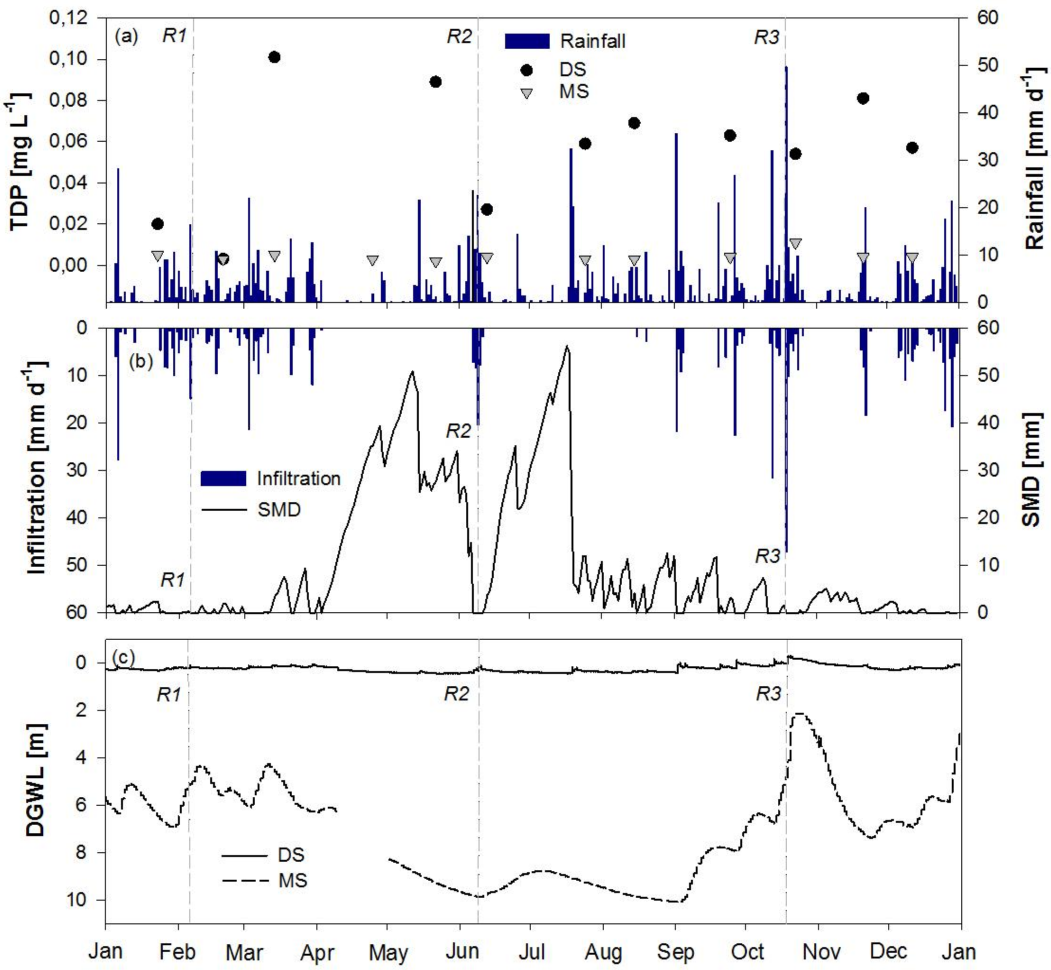


Figure 4: Evolution of (a) monthly groundwater TDP concentrations at sites DS (circle) and MS (square) and daily rainfall, (b) daily infiltration and soil moisture deficit and (c) depth to GWL over the study year 2017. Locations of the three study rainfall events (R1, R2 and R3) are also shown.

Rainfall event R1 [B; long duration with low total rainfall] occurred from the 6th to 7th of February, R2 [D; short duration with high total rainfall] from the 9th to 10th of June and R3 [E; long duration with high total rainfall] from the 18th to 19th of October. Event and pre-event characteristics are shown in **Figure 5**. Total rainfall was the highest for R3 and the smallest for R1 (50.6 and 19 mm, respectively), while maximum rainfall intensity was the smallest for R1 (3.2 mm $h^{-1}$) and comparable between R2 and R3 (6.2 and 6.4 mm $h^{-1}$, respectively).

Rainfall event R3 was the longest (40 h) while R2 was the shortest (15 h). Infiltration during the event was the highest for R3 and the lowest for R1 (47.1 and 16.8 mm, respectively). Pre-event total rainfall (previous 7 days) was the lowest for R1 (25.4 mm) and was comparable between R2 and R3 (55.8 and 57.2 mm, respectively).

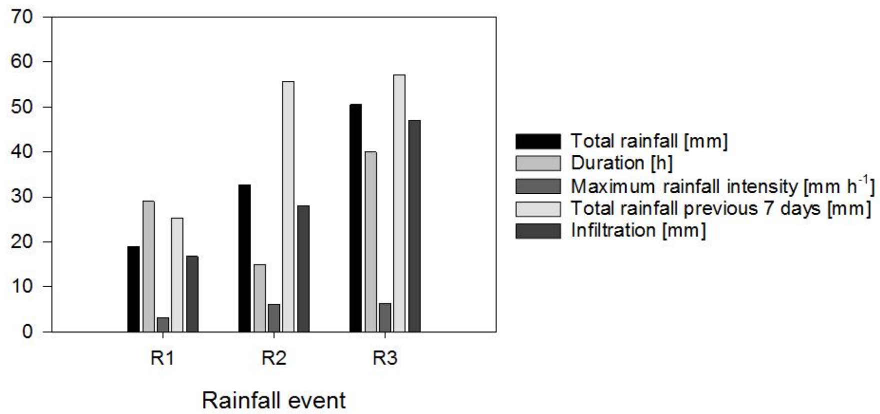


Figure 5: Summary of events and pre-events characteristics.

Daily SMD and infiltration for sites DS and MS (well-drained) over the year 2017 are shown in **Figure 4b**. Frequent rainfall from January to March and from September to December led to SMD less than 10 mm and frequent infiltration with an infiltration peak of 47 mm occurring in mid-October. From April to July, less rainfall led to increasing SMD with two SMD peaks in mid-May and mid-July above 50 mm. However, rainfall in late May - early June decreased SMD and led to infiltration in early June. Rainfall during July-August also decreased SMD but did not lead to infiltration, which occurred later in September. In total, 95 days of infiltration occurred during the year 2017, mainly between January and March (42 days), September and December (46 days) but also briefly in June (5 days) and August (2 days). Depth to GWL (DGWL) for both sites is shown in **Figure 4c**. At MS, DGWL was between 2 and 10 m with variations through the year. Depth to GWL increased in April (to reach 8-10 m) due to low rainfall and high SMD and remained high until September-October.

At this time of the year and until December, DGWL was lower due to low SMD and high rainfall leading to infiltration and GW recharge. At DS, DGWL was lower than at MS (up to 40 cm in April-September) with GWL sometimes above the ground level (September-December).

Over the year 2017, concentrations in TDP were higher at DS than at MS with variable concentrations at DS (**Fig. 4a**). In particular, TDP concentrations at DS were variable and on some occasions comparable to concentrations at MS between January and June whereas they remained elevated and were higher than at MS from July to December.

### 3.3. Modelled water flow

Modelled water flow breakthrough curves at the bottom of the DS and MS soil profiles are shown in **Figure 6** for each rainfall event R1 [B; long duration with low total rainfall] (**Fig. 6a**), R2 [D; short duration with high total rainfall] (**Fig. 6b**) and R3 [E; long duration with high total rainfall] (**Fig. 6c**). It should be noted that the upper boundary condition (atmospheric) was violated 63 % of the time for R3 at DS when the GWL was above ground level. The lower boundary condition (free drainage) was also violated at DS as the depth to GWL was less than 55 cm. Cumulative flow, flow first occurrence and flow peak timing and intensity are shown in **Table 5**. Modelled water mass balance was equal to 0.0 % indicating good performance of the models.

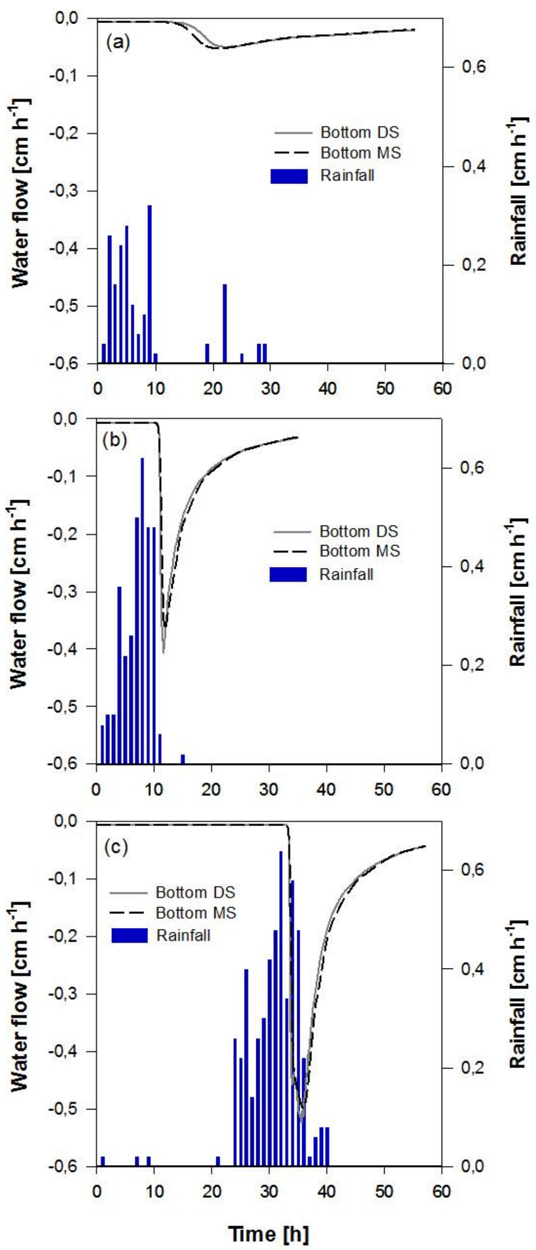


381

382 Figure 6: Water flow breakthrough curves at the bottom of the soil profiles DS and MS for

383 rainfall events (a) R1 [B; long duration with low total rainfall], (b) R2 [D; short duration with

384 high total rainfall] and (c) R3 [E; long duration with high total rainfall].

Table 5: Water flow breakthrough characteristics at sites DS and MS

for rainfall events R1, R2 and R3.

| Site | Rainfall event | Cumulative water flow [cm - % total rainfall] | Water flow first occurrence [h] | Water flow peak [h] | Water flow peak [cm $h^{-1}$] |
|---|---|---|---|---|---|
| **DS** | R1 | 1.4 – 74 % | 17 | 22.5 | 0.05 |
| | R2 | 2.5 – 76 % | 11 | 11.7 | 0.41 |
| | R3 | 4.0 – 78 % | 33 | 35.4 | 0.52 |
| **MS** | R1 | 1.5 – 79 % | 15 | 20.5 | 0.05 |
| | R2 | 2.5 – 76 % | 11 | 12.2 | 0.35 |
| | R3 | 4.1 – 80 % | 33 | 35.4 | 0.49 |

Cumulative water flow at the bottom of the soil profiles ranged from 74 to 80 % of total rainfall input and was similar between DS and MS during R2 and higher at MS than at DS during R1 and R3. Cumulative water flow was equal to 1.4, 2.5 and 4.0 cm at DS after rainfall events R1, R2 and R3, respectively. It was equal to 1.5, 2.5 and 4.1 cm at MS after these same events. First occurrence of water flow, resulting from the rainfall event, at the bottom of the soil profiles occurred at the same time for both sites DS and MS (during R2 and R3: after 11 and 33 h, respectively) or earlier at MS than at DS (during R1: after 17 and 15 h at DS and MS, respectively). Water flow peak occurred earlier at DS (11.7 h) than at MS (12.2 h) during R2 and earlier at MS (20.5 h) than at DS (22.5 h) during R1. Its intensity was similar between DS and MS during R1 and higher at DS (0.41 – 0.52 cm $h^{-1}$) than at MS (0.35 – 0.49 cm $h^{-1}$) during R2 and R3.

For both sites DS and MS, cumulative water flow was the lowest during R1 [B; long duration with low total rainfall] and the highest during R3 [E; long duration with high total rainfall].

Water flow first occurrence and flow peak occurred earlier during R2 [D; short duration with high total rainfall] and later during R3 where flow peak intensity was also the highest. Water flow peak intensity was the lowest during R1.

## 4. Discussion

This study investigated the spatial variability in water flow dynamics in soil profiles of two locations along a hillslope of contrasting GW P concentrations, and examined the inter-annual variability in water flow dynamics and GW P concentrations. A range of modelled soil hydraulic properties and subsurface water flow dynamics were identified to 1) determine static soil properties controlling water flow at different hillslope locations and 2) determine dynamic physical controls on temporal variations in water flow and shallow GW P concentrations to suggest potential mitigation strategies to reduce P transport to GW. The combined analysis of high resolution meteorological data, soil physical/hydraulic data and GW chemical data revealed contrasting spatial (soil) and temporal (rainfall, GWL) water flow dynamics, and subsequent P transport and attenuation potential, at different hillslope locations.

### 4.1. Spatial variability in subsurface water flow to groundwater

The potential for hydrological transport to GW varies within the same hillslope and is determined by soil physical and hydraulic properties, which also influence P sorption in the USZ and P transport to GW. The undisturbed soil cores studied suggested that the DS zone had a lower potential for hydrological transport than the MS zone due to a lower soil $K_s$, critical for water flow, despite its lower soil compaction (bulk density $\rho_b$) and higher soil $\phi$ and macroporosity. In contrast, the higher soil $K_s$ in the MS zone, and despite its higher soil $\rho_b$, lower soil $\phi$ and macroporosity, suggested a higher potential for vertical water flow in this zone (**Fig. 7**). However, water flow modelled at the bottom of the soil profiles using Hydrus 1D (**Fig. 6**) did not clearly reflected the differences in soil $K_s$ between DS and MS. Higher water flow peaks at DS (**Table 4**, **Fig. 6**) during high total rainfall events indicated the higher potential for water flow though the USZ at this site, even though water flow first occurrence did not appear earlier than at MS. In contrast, lower water flow peaks at MS (**Table 4**, **Fig. 6**) during high total rainfall events indicated the lower potential for water flow though the USZ at this site. Cumulative flow at the bottom of the soil profiles, lower at DS than at MS, and independently of the rainfall event (**Table 4**), reflected the differences in soil $\theta_s$ and soil water storage capacity which were higher at DS. However, as the depth to GWL was less than 55 cm at DS and was higher than 55 cm at MS, stronger differences in the timing and intensity of water flow reaching GW should be expected. High temporal resolution monitoring of GWL (**Fig. 4c**) also revealed a quick recharge of the aquifer at DS (although GWL is higher at this location) after rainfall events with a slow recovery to original water table positions whereas at MS response to rainfall was slower.

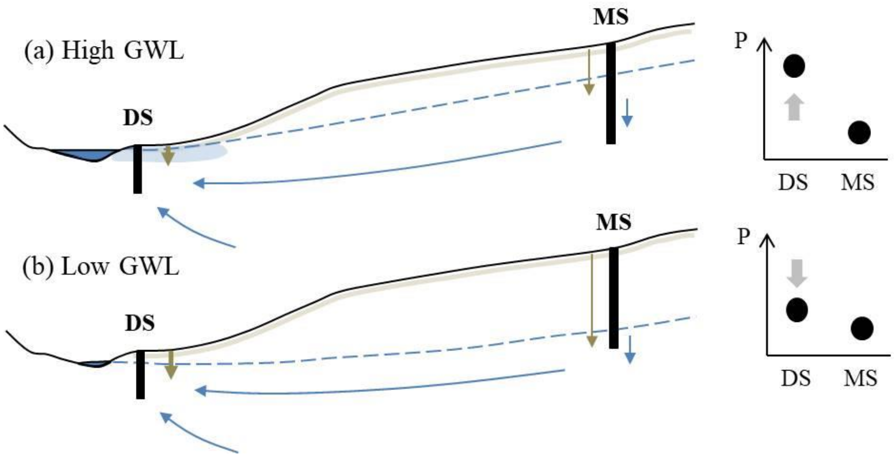


Figure 7: Schematic of contrasting groundwater P concentrations scenarios: (a) High GWL: contrasting concentrations between DS and MS with higher concentrations at DS due to the hydrological connection with soil P and (b) Low GWL: lower concentrations at DS and

similar to MS due to the hydrological disconnection with soil P. In both scenarios DS soil properties facilitate subsurface water flow to shallow GW.

Observed variability of soil hydraulic properties and water flow is supported to some extent by DeFauw et al. (2014) who observed no significant differences in infiltration dynamics between micro-topographic low position and high position. However, Hendrayanto et al. (1999) observed smaller soil $K_s$ at upper slope locations compared to mid-slope or down-slope locations, which has not been observed in this study and may be related to the high variability between replicates. Differences in soil texture and PSD, related to the slope position, may explain the differences of soil hydraulic properties between DS and MS, since hydraulic conductivities are coupled to the grain size distribution of soils (Mahmoodlu et al., 2016; Pachepsky and Rawls, 2003; Pachepsky et al., 2006). In this study, soil $\rho_b$ and $\phi$ were linked to soil PSD and indicated that sandy soils enhance water flow whereas clay soils attenuate it. Moreover, and even though both sites are under grassland with large root systems, the higher soil OM % at DS was reflected in the higher soil porosity which can be related to greater formation and hierarchy of aggregates (Daynes et al., 2013; Hirmas et al., 2013). Annual cropping activities with heavy machinery, more frequent in the MS zone (fertilization, grass harvesting, grazing) than in the DS zone (grazing, fertilization), can also contribute to the higher soil $\rho_b$, lower soil macroporosity (Pagliai et al., 2004) and soil OM % (Franzluebbers et al., 2014; Gimenez et al., 2002) observed at MS and influence water infiltration.

However, this study focused only on the first 55 cm of soil and incorporated some uncertainties regarding the vertical variations of soil hydraulic properties at DS where two consecutive horizons were assumed to be similar to model water flow. It is also difficult to estimate water flow reaching GW in the MS zone where the GW table is deeper. Further work is needed to better understand the vertical physical heterogeneity of the deeper soil, especially where the GW table is deeper. Despite these limitations, the results indicate that there is less time for P sorption to occur in the DS zone as water flow is a quicker process. Interaction between soil solution P and the soil matrix is also likely reduced due to more water flowing *via* macropores and bypassing the sorption sites at DS. These hypotheses should be further investigated by incorporating soil chemical data in the models to account for P transport including colloidal P. Mitigation strategies to reduce GW P concentrations should prioritize the DS zone even though deeper GW flowpaths from the MS zone or upslope could be a potential source of P to the DS zone.

### 4.2. Inter-annual variability in subsurface water flow to groundwater

The potential for hydrological transport to GW, and subsequent P transport, also varied within the same hillslope zone and appeared to be linked to the inter-annual dynamic of other physical controls such as rainfall and GWL, as observed over the year 2017. Modelling of water flow at the bottom of the soil profiles during contrasting rainfall events using Hydrus 1D showed that rainfall pattern influenced water flow. It was flashier with higher flow peaks during the high total rainfall events than during the low total rainfall event which suggested less time for P attenuation processes to occur when water flows during short and intense rainfall events and during longer rainfall events of autumn-winter leading to higher GW P concentrations.

Moreover, seasonal variations in GW P concentrations revealed at the DS zone by monthly monitoring appeared to be controlled by GWL fluctuations. Shallower GW (August – December) (**Fig. 4c, Fig. 7a**) may lead to lower water flow travel time through the USZ, compared to dry periods where the GWL is deeper, and further reduce P attenuation processes. It may also lead to reductive dissolution of soil Fe hydroxides being solubilised as $Fe^{2+}$ and releasing P previously adsorbed (Vidon et al., 2010). This can be important in the DS zone where shallow GW can connect with and mobilise a higher soil P source as chemical tests on composite soil samples revealed a higher soil labile inorganic P content (90 mg $kg^{-1}$) and DPS (8.3 %) at DS than at the MS (45 mg $kg^{-1}$ and 4.0 %, respectively) (Fresne et al., 2020), where GWL is also deeper. Previous GW monitoring also showed low $N\text{-}NO_3^-$ concentration (mean annual concentrations of 0.03 ± 0.01 mg $L^{-1}$) due to denitrifying conditions (mean annual ORP of 6.0 ± 1.8 mV) (McAleer et al., 2017) and higher Fe (4712 ± 1526 µg $L^{-1}$) and Mn (2928 ± 197 mg $L^{-1}$) concentrations at DS than at MS; this supports the hypothesis of Fe oxyhydroxide reduction. Organic riparian soils are known as internal sources of soluble reactive P (Dupas et al., 2017b; Gu et al., 2017; Records et al., 2016) due to poor retention capacities (Daly et al., 2001; Roberts et al., 2017) and where soil solution P concentrations have been strongly linked to GWL dynamics (Dupas et al., 2015). In contrast, hydrochemical GW data at MS revealed nitrification processes (mean annual ORP of 162.5 ± 3.5 mV) occurring (McAleer et al., 2017). This site had higher annual mean $N\text{-}NO_3^-$ concentration (7.21 ± 0.38 mg $L^{-1}$) but lower Fe (3.85 ± 0.87 µg $L^{-1}$) and Mn concentrations (2.87 ± 0.74 mg $L^{-1}$) than at DS. This suggests that reduction of Fe hydroxides is limited and may support lower GW P concentrations measured at this site. However, as the GW table sinks during dry periods in the DS zone in April, or later in the year in the MS zone (**Fig. 7b**), it may leave the higher P sources in the topsoil disconnected and increase water flow travel time enhancing P attenuation processes.

However, P concentrations measured in GW can result from a combination of vertical P leaching from soil and lateral flows within the aquifer transporting P from the upper hillslope which are not considered here. Further work is needed including acquisition of higher resolution GW chemical data to get a better understanding of the main processes explaining inter-annual P dynamics, especially in the near stream zone DS. Inclusion of the different P species and fractions, including colloidal P (1-1000 nm), would be an important improvement into understanding such processes. Remediation measures should prioritise reducing soil P source at DS by limiting the timing and/or the intensity of grazing especially during periods of higher GWL that may mobilise P. Reduction of P applications (as synthetic or organic fertilizers) on the MS zone and the upslope should also be considered.

## 5. Conclusion

Both static and dynamic factors influence water flow through the USZ to shallow GW, controlling soil P attenuation processes, and can therefore contribute to spatial and temporal variations in GW P concentrations. In this study, two conceptual views of the hillslope emerged. The first corresponds to variable concentration at DS, on some occasions low and similar to concentrations at MS, due to less connection between GW and soil P (lower GWL), slower water flow and longer water travel time to GW, even though the DS zone has more potential for hydrological transport than the MS zone due to its soil physical properties. The second corresponds to contrasting concentrations between DS and MS with DS becoming temporally elevated due to the hydrological connection with soil P (higher GWL), flashier water flow and shorter water travel time to GW. Hence, soil physical and hydraulic properties control water flow and travel time to GW, and subsequent P transport to GW, and should be considered to better target cost-effective mitigation measures. Reduction of P sources (from grazing or fertilization) should be prioritized in zones of higher potential for hydrological transport or shallow GWL as the near-stream zones.

## Author contribution

MF: Conceptualization, Methodology, Validation, Formal analysis, Investigation, Data curation, Writing – original draft, Writing – reviewing and editing, Visualization. OF: Conceptualization, Methodology, Validation, Resources, Writing – reviewing and editing, Supervision. PEM: Conceptualization, Methodology, Resources, Writing – reviewing and editing, Funding acquisition. PJ and KD: Conceptualization, Methodology, Writing – reviewing and editing.

## Competing interests

The authors declare that they have no conflict of interest.

## Acknowledgements

We thank the ACP land owners and farmers of the fields for cooperation and sampling permission, the ACP staff especially David Ryan and Dermot Leahy for field sampling assistance, Una Cullen for meteorological and GW level data supply. The lab work of Shane Scannell for bulk density analyses is greatly appreciated. We also thank Matthias Bacher for Hyprop training and Cathal Somers for help in Hyprop lab set up and particle size analyses. Funding was provided by the Department of Agriculture, Food and the Marine through the Teagasc Agricultural Catchments Programme and by the Teagasc Walsh Fellowship Programme.

## References

Agah, A. E., Meire, P., and Deckere, E.: Simulation of phosphorus transport in soil under municipal wastewater application using hydrus-1D. In: Soil contaminations - Current consequences and further solutions, InTech, 177-190, 2016.

Anderson, A. E., Weiler, M., Alila, Y., and Hudson, R. O.: Dye staining and excavation of a lateral preferential flow network, Hydrol. Earth Syst. Sci., 13, 935–944, 2009.

Askew, F. E.: Persulfate method for simultaneous determination of total nitrogen and total phosphorus. 4500-P J, in: Eaton, A. D., Clesceri, L. S., Rice, W. E., and Greenberg, A. E., editors. Standard Methods for the Examination of Water and Wastewater, 21st edition. ISBN 0-87553-047-8. 800 1 street, NW Washington, DC 2001-3710: American Public Health Association, 160-161, 2005.

Askew, F. E. and Smith, R. K.: Inorganic non metallic constituents; Phosphorus; Method 4500-P F. Automated ascorbic acid reduction method, in: Eaton, D. A., Clesceri, L. S., Rice, E. W., and Greensberg, A. E., editors. Standard Methods for the Examination of Waters and Waste Water. 800 1 street, NW Washington, DC 2001-3710: ISBN 0-87553-047-8 American Public Health Association, 4-155, 2005.

Avery, B. W. and Bascomb, C. L.: Soil survey laboratory methods.: Soil Survey of Great Britain (England and Wales), Harpenden (Rothamsted Experimental Station, Harpenden, Herts.), 1974.

Bacher, M. G., Schmidt, O., Bondi, G., Creamer, R., and Fenton, O.: Comparison of Soil Physical Quality Indicators Using Direct and Indirect Data Inputs Derived from a Combination of In-Situ and Ex-Situ Methods, Soil Science Society of America Journal, 83, 5-17, 2019.

Bachmair, S. and Weiler, M.: Hillslope characteristics as controls of subsurface flow variability, Hydrol. Earth Syst. Sci., 16, 3699–3715, 2012a.

Bachmair, S., Weiler, M., and Troch, P. A.: Intercomparing hillslope hydrological dynamics: spatio–temporal variability and vegetation cover effects, Water Resour. Res., 48, 2012b.

Bezerra-Coelho, C. R., Zhuang, L., Barbosa, M. C., Soto, M., and van Genuchten, M. T.: Further tests of the HYPROP evaporation method for estimating the unsaturated soil hydraulic properties, Journal of Hydrology and Hydromechanics, 66(2), 161-169, 2018.

Bol, R., Julich, D., Brödlin, D., Siemens, J., Kaiser, K., Dippold, M. A. et al.: Dissolved and colloidal phosphorus fluxes in forest ecosystems—an almost blind spot in ecosystem research, J Plant Nutr Soil Sci., 179, 425-438, 2016.

Brady, N.C. and Weil, R. R.: The Nature and Properties of Soils, 14th Edition. United States of America: Pearson Education Inc., 2008.

Bünemann, E. K., Bongiorno, G., Bai, Z., Creamer, R. E., De Deyn, G., de Goede, R. et al.: Soil quality – A critical review, Soil Biology and Biochemistry, 120, 105-125, 2018.

Cordell, D. and White, S.: Life's Bottleneck: Sustaining the World's Phosphorus for a Food Secure Future, Annual Review of Environment and Resources, 39, 161, 2014.

Daly, K., Jeffrey, D., and Tunney, H.: The effect of soil type on phosphorus sorption capacity and desorption dynamics in Irish grassland soils, Soil Use Manage., 17, 12-20, 2001.

Daynes, C. N., Field, D. J., Saleeba, J. A., Cole, M. A., and McGee, P. A.: Development and stabilisation of soil structure via interactions between organic matter, arbuscular mycorrhizal fungi and plant roots, Soil biology & biochemistry, 57, 683-694, 2013.

DeFauw, S. L., Brye, K. R., Sauer, T. J., and Hays, P.: Hydraulic and Physiochemical Properties of a Hillslope Soil Assemblage in the Ozark Highlands, Soil Sci., 179(3), 107-117, 2014.

Duan, J., Yang, J., Tang, C., Chen, L., Liu, Y., and Wang, L.: Effects of rainfall patterns and land cover on the subsurface flow generation of sloping Ferralsols in southern China, PLOS ONE, 12(8), 2017.

Dupas, R., Gruau, G., Gu, S., Humbert, G., Jaffrézic, A., and Gascuel-Odoux, C.: Groundwater control of biogeochemical processes causing phosphorus release from riparian wetlands, Water Research, 84, 307-314, 2015.

Dupas, R., Mellander, P-E., Gascuel-Odoux, C., Fovet, O., McAleer, E. B., McDonald, N. T. et al.: The role of mobilisation and delivery processes on contrasting dissolved nitrogen and phosphorus exports in groundwater fed catchments, Science of The Total Environment, 599-600, 1275-1287, 2017a.

Dupas, R., Musolff, A., Jawitz, J. W., Rao, P. S. C., Jäger, C. G., Fleckenstein, J. H. et al.: Carbon and nutrient export regimes from headwater catchments to downstream reaches, Biogeosciences, 14, 4391–4407, 2017b.

Durner, W.: Hydraulic conductivity estimation for soils with heterogeneous pore structure, Water Resour Res., 30, 211-223, 1994.

Elmi, A., Abou Nohra, J. S., Madramootoo C. A., and Hendershot, W.: Estimating phosphorus leachability in reconstructed soil columns using HYDRUS-1D model, Environ Earth Sci, 65, 1751-1758, 2012.

Fealy, R. M., Buckley, C., Mechan, S., Melland, A., Mellander, P-E., Shortle, G. et al.: The Irish Agricultural Catchments Programme: catchment selection using spatial multi-criteria decision analysis, Soil Use Manage., 26, 225-236, 2010.

Fenton, O., Vero, S., Ibrahim, T. G., Murphy, P. N. C., Sherriff, S. C., and Ó hUallacháin, D.: Consequences of using different soil texture determination methodologies for soil physical quality and unsaturated zone time lag estimates, Journal of Contaminant Hydrology, 182, 16-24, 2015.

Fenton, O., Mellander, P-E., Daly, K., Wall, D. P., Jahangir, M. M. R., Jordan, P. et al.: Integrated assessment of agricultural nutrient pressures and legacies in karst landscapes, Agriculture, Ecosystems & Environment, 239, 246-256, 2017.

Franzluebbers, A. J., Sawchik, J., and Taboada, M. A.: Agronomic and environmental impacts of pasture–crop rotations in temperate North and South America, Agriculture, ecosystems & environment, 190, 18-26, 2014.

Fresne, M., Jordan, P., Fenton, O., Mellander, P-E., and Daly, K.: Soil chemical and fertilizer influences on soluble and medium-sized colloidal phosphorus in agricultural soils, Science of the total environment, 142112, 2020.

Fuchs, J. W., Fox, G. A., Storm, D. E., Penn, C. J., and Brown, G. O.: Subsurface Transport of Phosphorus in Riparian Floodplains: Influence of Preferential Flow Paths, Journal of Environmental Quality, 38(2), 473-484, 2009.

Gao, Y., Zhu, B., Wang, T., Tang, J. L., Zhou, P., and Miao, C. Y.: Bioavailable phosphorus transport from a hillslope cropland of purple soil under natural and simulated rainfall, Environmental Monitoring and Assessment, 171, 539-550, 2010.

Giménez, D., Karmon, J. L., Posadas, A., and Shaw, R. K.: Fractal dimensions of mass estimated from intact and eroded soil aggregates, Soil & tillage research, 64, 165-172, 2002.

Gladnyeva, R. and Saifadeen, A. Effects of hysteresis and temporal variability in meteorological input data in modelling of solute transport in unsaturated soil using Hydrus-1D, Journal Of Water Resources Planning And Management, 68, 285-293, 2013.

Gottler, R. A., and Piwoni, M. D.: Metals. Method 3120 B. Inductively coupled plasma (ICP) method, in: Eaton, D. A., Clesceri, L. S., Rice, E. W., and Greensberg, A. E., editors. Standard Methods for the Examination of Waters and Waste Water. 21st ed. 800 1 street, NW Washington, DC 2001-3710: American Public Health Association, 3-39, 2005.

Graham, C. B., Woods, R. A., and McDonnell, J. J.: Hillslope threshold response to rainfall: (1) A field based forensic approach, J. Hydrol., 393, 65–76, 2010.

Gu, S., Gruau, G., Dupas, R., Rumpel, C., Crème, A., Fovet, O. et al.: Release of dissolved phosphorus from riparian wetlands: Evidence for complex interactions among hydroclimate variability, topography and soil properties, Science of The Total Environment, 598, 421-431, 2017.

Guo, L., Lin, H., Fan, B., Nyquist, J., Toran, L., and Mount, G. J.: Preferential flow through shallow fractured bedrock and a 3D fill-and-spill model of hillslope subsurface hydrology, Journal of Hydrology, 576, 430-442, 2019.

Hendrayanto, Kosugi, K., Uchida, T., Matsuda, S., and Mizuyama, T.: Spatial Variability of Soil Hydraulic Properties in a Forested Hillslope, J For Res, 4, 107-114, 1999.

Hirmas, D. R., Giménez, D., Subroy, V., Platt, B. F.: Fractal distribution of mass from the millimeter- to decimeter-scale in two soils under native and restored tallgrass prairie, Geoderma, 207-208, 121-130, 2013.

Ibrahim, T. G., Fenton, O., Richards, K. G., Fealy, R. M., and Healy, M. G.: Spatial and temporal variations of nutrient loads in overland flow and subsurface drainage from a marginal land site in south-east Ireland, Biology and Environment: Proceedings of the Royal Irish Academy, 113B(2), 1-18, 2013.

Jacques, D., Šimůnek, J., Mallants, D., and van Genuchten, M. T.: Modelling coupled water flow, solute transport and geochemical reactions affecting heavy metal migration in a podzol soil, Geoderma, 145, 449-461, 2008.

Julich, D., Julich, S., and Feger, K.: Phosphorus fractions in preferential flow pathways and soil matrix in hillslope soils in the Thuringian Forest (Central Germany), J Plant Nutr Soil Sci., 180, 407-417, 2017.

Kamphake, L. J., Hannah, S. A., and Cohen, J. M.: Automated analysis for nitrate by hydrazine reduction, Water Res., 1, 205-216, 1967.

Kurz, I., Coxon, C., Tunney, H., and Ryan, D.: Effects of grassland management practices and environmental conditions on nutrient concentrations in overland flow, Journal of Hydrology, 304, 35-50, 2005.

Lehmann, P., Hinz, C., McGrath, G., Tromp-van-Meerveld, H. J., and McDonnell, J. J.: Rainfall threshold for hillslope outflow: an emergent property of flow pathway connectivity, Hydrol. Earth Syst. Sci., 11, 1047-1063, 2007.

Lintern, A., Webb, J. A., Ryu, D., Liu, S., Bende-Michl, U., Waters, D. et al.: Key factors influencing differences in stream water quality across space. WIREs Water, 5: e1260, 2018.

Mabilde, L., De Neve, S., and Sleutel, S.: Regional analysis of groundwater phosphate concentrations under acidic sandy soils: Edaphic factors and water table strongly mediate the soil P-groundwater P relation, Journal of Environmental Management, 203(1), 429-438, 2017.

Mahmoodlu, M. G., Raoof, A., Sweijen, T., and van Genuchten, M. T.: Effects of Sand Compaction and Mixing on Pore Structure and the Unsaturated Soil Hydraulic Properties, Vadose Zone Journal, 15(8), 2016.

McAleer, E. B., Coxon, C. E., Richards, K. G., Jahangir, M. M. R., Grant, J., and Mellander, P-E.: Groundwater nitrate reduction versus dissolved gas production: A tale of two catchments, Science of The Total Environment, 586, 372-389, 2017.

McGinley, P. M., Masarik, K. C., Gotkowitz, M. B., and Mechenich, D. J.: Impact of anthropogenic geochemical change and aquifer geology on groundwater phosphorus concentrations, Applied Geochemistry, 72, 1-9, 2016.

Melland, A. R., Mellander, P-E., Murphy, P. N. C., Wall, D. P., Mechan, S., Shine, O. et al.: Stream water quality in intensive cereal cropping catchments with regulated nutrient management, Environmental Science & Policy, 24, 58-70, 2012.

Mellander, P-E., Melland, A. R., Murphy, P. N. C., Wall, D. P., Shortle, G., and Jordan, P.: Coupling of surface water and groundwater nitrate-N dynamics in two permeable agricultural catchments, The Journal of Agricultural Science, 152, 107-124, 2014.

Mellander, P-E., Jordan, P., Shore, M., McDonald, N. T., Wall, D. P., Shortle, G. et al.: Identifying contrasting influences and surface water signals for specific groundwater phosphorus vulnerability, Science of The Total Environment, 541, 292-302, 2016.

Mellander, P-E., Jordan, P., Bechmann, M., Fovet, O., Shore, M., McDonald, N. T. et al. Integrated climate-chemical indicators of diffuse pollution from land to water, Scientific Reports, 8, 944, 2018.

Mualem, Y.: A new model for predicting the hydraulic conductivity of unsaturated porous media, Water Resour Res., 12, 513-522, 1976.

Neidhard, H., Schoeckle, D., Schleinitz, A., Eiche, E., Berner, Z., Tram, P. T. K. et al.: Biogeochemical phosphorus cycling in groundwater ecosystems – Insights from South and Southeast Asian floodplain and delta aquifers, Science of the Total Environment, 644, 1357-1370, 2018.

Pachepsky, Y. A. and Rawls, W. J.: Soil structure and pedotransfer functions, Eur J Soil Sci., 54, 443-452, 2003.

Pachepsky, Y. A., Rawls, W. J., and Lin, H. S.: Hydropedology and pedotransfer functions, Geoderma, 131, 308-316, 2006.

Pagliai, M., Vignozzi, N., and Pellegrini, S.: Soil structure and the effect of management practices, Soil & tillage research, 79, 131-143, 2004.

Pang, L., Lafogler, M., Knorr, B., McGill, E., Saunders, D., Baumann, T. et al.: Influence of colloids on the attenuation and transport of phosphorus in alluvial gravel aquifer and vadose zone media, Science of The Total Environment, 550, 60-68, 2016.

Pferdmenges, J., Breuer, L., Julich, S., and Kraft, P.: Review of soil phosphorus routines in ecosystem models, Environmental modelling & software : with environment data news, 126, 104639, 2020.

Radcliffe, D. E., Reid, D. K., Blombäck, K., Bolster, C. H., Collick, A. S., Easton, Z. M. et al.: Applicability of Models to Predict Phosphorus Losses in Drained Fields: A Review, Journal of environmental quality, 44, 614-628, 528.

Records, R. M., Wohl, E., and Arabi M.: Phosphorus in the river corridor, Earth-Science Reviews, 158, 65-88, 2016.

Roberts, W. M., Gonzalez-Jimenez, J. L., Doody, D. G., Jordan, P., and Daly, K.: Assessing the risk of phosphorus transfer to high ecological status rivers: Integration of nutrient management with soil geochemical and hydrological conditions, Science of The Total Environment, 589, 25-35, 2017.

Schilling, K. E., Kim, S., Jones, C. S., and Wolter, C. F.: Orthophosphorus Contributions to Total Phosphorus Concentrations and Loads in Iowa Agricultural Watersheds, Journal of Environmental Quality, 46(4), 828-835, 2017.

Schoumans, O. F. and Groenendijk, P.: Modeling Soil Phosphorus Levels and Phosphorus Leaching From Agricultural Land In the Netherlands, Journal of environmental quality, 29(1), 111-116, 2000.

Schoumans, O. F., Silgram, M., Groenendijk, P., Bouraoui, F., Andersen, H. E., Kronvang, B. et al. Description of nine nutrient loss models: capabilities and suitability based on their characteristics, Journal of Environmental Monitoring, 11(3), 5066-5114, 2009.

Schulte, R. P. O., Diamond, J., Finkele, K., Holden, N. M., and Brereton, A. J.: Predicting the soil moisture conditions of Irish grassland, Irish Journal of Agriculture and Food Research, 44(1), 95-110, 2005.

Sharpley, A. N.: Managing agricultural phosphorus to minimize water quality impacts, Scientia Agricola, 73(1), 1-8, 2016.

Šimůnek, J., van Genuchten, M. T., and Sejna, M.: Modeling subsurface water flow and solute transport with HYDRUS and related numerical software packages. In: Navarro PG, Playán E, editors. Numerical Modelling of Hydrodynamics for Water Resources., 2008.

Šimůnek, J., Šejna, M., Saito, H., Sakai, M, and van Genuchten, M. T.: The HYDRUS 1D software package for simulating the movement of water, heat and multiple solutes in variably saturated media. Version 4.16 HYDRUS software series Riverside, California, USA.: Department of Environmental Science, University of California Riverside, 2013.

Sinha, E., Michalak, A. M., and Balaji, V.: Eutrophication will increase during the 21st century as a result of precipitation changes, Science, 357, 407-408, 2017.

Tromp-van Meerveld, H. J. and Weiler, M.: Hillslope dynamics modeled with increasing complexity, J. Hydrol., 361, 24–40, 2008.

van Genuchten, M. T.: A Closed-form Equation for Predicting the Hydraulic Conductivity of Unsaturated Soils, Soil Science Society of America journal, 44, 892-898, 1980.

Vereecken, H., Javaux, M., Weynants, M., Pachepsky, Y., Schaap, M., and van Genuchten, M. T.: Using pedotransfer functions to estimate the van genuchten- mualem soil hydraulic properties: A review, Vadose Zone Journal, 9(4), 795-820, 2010.

Vero, S. E., Ibrahim, T. G., Creamer, R. E., Grant, J., Healy, M. G., Henry, T. et al.: Consequences of varied soil hydraulic and meteorological complexity on unsaturated zone time lag estimates, Journal of Contaminant Hydrology, 170, 53-67, 2014.

Vidon, P., Allan, C., Burns, D., Duval, T. P., Gurwick, N., Inamdar, S. et al.: Hot Spots and Hot Moments in Riparian Zones: Potential for Improved Water Quality Management, Journal of the American Water Resources Association, 46, 278-298, 2010.

Wilson, G. V., Jardine, P. M., Luxmoore, R. J., and Jones, J. R.: Hydrology of a forested hillslope during storm events.,Geoderma ,46, 119-138, 1990.

Wilson, G. V., Nieber, J. L., Fox, G. A., Dabney, S. M., Ursic, M., and Rigby, J. R.: Hydrologic connectivity and threshold behavior of hillslopes with fragipans and soil pipe networks, Hydrol Process, 31, 2477-2496, 2017.

Withers, P. J. A., Neal, C., Jarvie, H. P., and Doody, D. G.: Agriculture and Eutrophication: Where Do We Go from Here?, Sustainability, 6, 5853-5875, 2014.